

Properties of B_4C-TiB_2 ceramics prepared by spark plasma sintering

Jingzhe Fan(范静哲), Weixia Shen(沈维霞), Zhuangfei Zhang(张壮飞), Chao Fang(房超), Yuewen Zhang(张跃文), Liangchao Chen(陈良超), Qianqian Wang(王倩倩), Biao Wan(万彪), and Xiaopeng Jia(贾晓鹏)
Citation: Chin. Phys. B, 2021, 30 (**3**): 038105. DOI: 10.1088/1674-1056/abd7d8
Journal homepage: http://cpb.iphy.ac.cn; http://iopscience.iop.org/cpb

What follows is a list of articles you may be interested in

Effects of heat transfer in a growing particle layer on microstructural evolution during solidification of colloidal suspensions

Jia-Xue You(游家学), Yun-Han Zhang(张运涵), Zhi-Jun Wang(王志军), Jin-Cheng Wang(王锦程), and Sheng-Zhong Liu(刘生忠)
Chin. Phys. B, 2021, 30 (**2**): 028103. DOI: 10.1088/1674-1056/abc168

A review of experimental advances in twisted graphene moirè superlattice

Yanbang Chu(褚衍邦), Le Liu(刘乐), Yalong Yuan(袁亚龙), Cheng Shen(沈成), Rong Yang(杨蓉), Dongxia Shi(时东霞), Wei Yang(杨威), and Guangyu Zhang(张广宇)
Chin. Phys. B, 2020, 29 (**12**): 128104. DOI: 10.1088/1674-1056/abb221

A systematic study of light dependency of persistent photoconductivity in a-InGaZnO thin-film transistors

Yalan Wang(王雅兰), Mingxiang Wang(王明湘), Dongli Zhang(张冬利), and Huaisheng Wang(王槐生)
Chin. Phys. B, 2020, 29 (**11**): 118101. DOI: 10.1088/1674-1056/abb222

Construction of monolayer $IrTe_2$ and the structural transition under low temperatures

Aiwei Wang(王爱伟), Ziyuan Liu(刘子媛), Jinbo Pan(潘金波), Qiaochu Li(李乔楚), Geng Li(李更), Qing Huan(郇庆), Shixuan Du(杜世萱), Hong-Jun Gao(高鸿钧)
Chin. Phys. B, 2020, 29 (**7**): 078102. DOI: 10.1088/1674-1056/ab90eb

Optical and electrical properties of InGaZnON thin films

Jian Ke Yao(姚建可), Fan Ye(叶凡), Ping Fan(范平)
Chin. Phys. B, 2020, 29 (**1**): 018105. DOI: 10.1088/1674-1056/ab5fc1

Properties of B_4C-TiB_2 ceramics prepared by spark plasma sintering*

Jingzhe Fan(范静哲), Weixia Shen(沈维霞), Zhuangfei Zhang(张壮飞)†,
Chao Fang(房超), Yuewen Zhang(张跃文), Liangchao Chen(陈良超)‡,
Qianqian Wang(王倩倩), Biao Wan(万彪), and Xiaopeng Jia(贾晓鹏)§

Key Laboratory of Material Physics, Ministry of Education, School of Physics and Microelectronics, Zhengzhou University, Zhengzhou 450052, *China*

(Received 7 October 2020; revised manuscript received 25 November 2020; accepted manuscript online 4 January 2021)

By doping titanium hydride (TiH_2) into boron carbide (B_4C), a series of B_4C+x wt% TiH_2 ($x=0$, 5, 10, 15, and 20) composite ceramics were obtained through spark plasma sintering (SPS). The effects of the sintering temperature and the amount of TiH_2 additive on the microstructure, mechanical and electrical properties of the sintered B_4C-TiB_2 composite ceramics were investigated. Powder mixtures of B_4C with 0–20 wt% TiH_2 were heated from 1400 °C to 1800 °C for 20 min under 50 MPa. The results indicated that higher sintering temperatures contributed to greater ceramic density. With increasing TiH_2 content, titanium diboride (TiB_2) formed between the TiH_2 and B_4C matrix. This effectively improved Young's modulus and fracture toughness of the composite ceramics, significantly improving their electrical properties: the electrical conductivity reached 114.9 S·cm^{-1} at 1800 °C when $x=20$. Optimum mechanical properties were obtained for the B_4C ceramics sintered with 20 wt% TiH_2, which had a relative density of 99.9±0.1%, Vickers hardness of 31.8 GPa, and fracture toughness of 8.5 MPa·m$^{1/2}$. The results indicated that the doping of fine Ti particles into the B_4C matrix increased the conductivity and the fracture toughness of B_4C.

Keywords: boron carbide ceramics, conductivity, hardness, fracture toughness

PACS: 81.05.Je, 61.72.U–, 81.20.Ev, 81.65.Ps **DOI:** 10.1088/1674-1056/abd7d8

1. Introduction

With developments in science and technology, the research and application of ceramic composite materials have attracted increasing attention. Furthermore, due to the electrical conductivity of ceramics, they can be widely used as high-temperature electrothermal elements in oxidizing atmospheres, as cathodes in high-temperature fuel cells and as electrodes for magnetohydrodynamic power generation.[1,2] Traditional conductive ceramic materials, whether oxide or non-oxide ceramic materials, have low conductivity at room temperature. Therefore, the synthesis of conductive super-hard materials at room temperature would not only be of great scientific significance but also of great value for expanding the applications of ceramic materials.

The third hardest material known to man, black diamond, or B_4C ceramic,[3–6] is an attractive ceramic because of its excellent properties such as low density (2.51 g·cm^{-3}), high melting point (2447 °C), high hardness (29–31 GPa), outstanding chemical stability, and excellent absorption neutron cross-section (600 b). It has many applications, such as abrasive cutting, as a coating material, for light-weight armor, and for controlling nuclear fission.[7,8] B_4C ceramic also has high Young's modulus (390–440 GPa) and low fracture toughness (2.16–2.52 MPa·m$^{1/2}$).[9,10] Due to these characteristics, B_4C ceramic is too difficult to sinter. B_4C ceramic with high density can be obtained by pressureless sintering or hot pressing at above 2200 °C, however these conditions not only enable the grains to grow too easily but also waste thermal energy, which greatly limits B_4C ceramic application.[11,12]

TiB_2 is another super-hard material with high hardness (34 GPa) and excellent electrical conductivity (14.4 μΩ·cm). It can be combined with B_4C to form a composite material that results in inhibition of grain growth, lower sintering temperature, and improved mechanical properties.[13–19] When sintered at high temperature, the overall performance of nanoscale Ti and B_4C powders is weaker than that of pure B_4C.[20] Additionally, Ti is easily oxidized into Ti–O phase, or Ti–B–O and Ti–C–O solid solutions. Nanoscale Ti powers are usually unstable, so they are too difficult to handle. Therefore, TiH_2 has been used to disperse Ti particles in the B_4C ceramic matrix to synthesize TiB_2, thereby optimizing its performance.[21] The fabrication of B_4C-TiB_2 composite ceramics using B_4C and TiH_2 as starting materials by the spark plasma sintering (SPS) method has not yet been reported. In the SPS process, the sintering is carried out at lower temperature and the process proceeds faster than conventional processes thanks to the use of pulse current for heating the powders to be sintered. Besides, spark discharges are ignited in the pores during a current pulse, which can efficiently remove the adsorbed gases and oxides from the powder particle sur-

*Project supported by the National Natural Science Foundation of China (Grant Nos. 11704340 and 11804305) and the Scientific and Technology Project in Henan Province, China (Grant No. 202102210198).

†Corresponding author. E-mail: zhangzf@zzu.edu.cn

‡Corresponding author. E-mail: chenlc@zzu.edu.cn

§Corresponding author. E-mail: xpjia@zzu.edu.cn

© 2021 Chinese Physical Society and IOP Publishing Ltd

faces, thereby facilitating the formation of active contacts between them.[22] The main aim of the present work is to synthesize B_4C-TiB_2 composite ceramics and investigate the effect of TiH_2 powders on the B_4C ceramic properties.

2. Materials and methods

B_4C powder (99.5%, 1–10 μm) and TiH_2 powder (99%, −325 mesh) were purchased from Shanghai Aladdin Biochemical Technology, Shanghai, China and used as the starting materials.[23] Figure 1 shows the microstructures of these two raw materials. Powders composed of B_4C and TiH_2 (0, 5, 10, 15, 20 wt%) were mixed for more than 30 min in an agate mortar and then put into a graphite die (40 mm in depth and 13.1 mm in diameter). The die was lined with graphite paper to separate the powders from graphite mould. The mixtures were sintered by SPS (LABOX-325R, Sinter Land Inc, Japan) under a uniaxial pressure of 50 MPa in a vacuum. A schematic diagram of the sample preparation process and SPS is shown in Fig. 2. By using a two-stage heating process, TiH_2[24–26] was first completely decomposed at 800 °C for 10 min and then heated to 1400 °C, 1500 °C, 1600 °C, 1700 °C, and 1800 °C for 20 min, each, at a heating rate of 100 °C·min^{-1}. Figure 3 shows the temperature and displacement changes of the sample during 1800 °C sintering, revealing that the sample had a positive displacement and indicating that the sample was gradually densified.

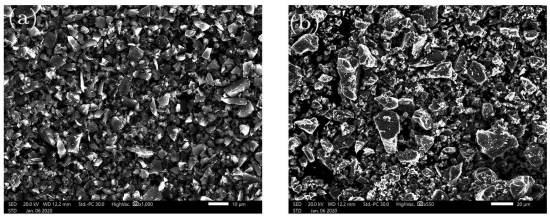


Fig. 1. Microstructure of (a) B_4C and (b) TiH_2 powders.

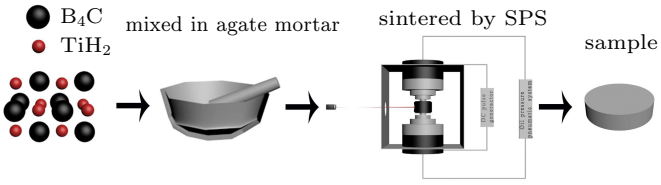


Fig. 2. The procedure of sample sintering.

After polishing the sintered B_4C-TiB_2 composite ceramics, their density was determined using the Archimedes displacement method. The microstructures of the composite ceramics were characterised by x-ray diffraction (XRD; X-pert, Japan) using Cu-$K\alpha$ radiation ($\lambda = 1.5406$ Å) and scanning electron microscopy (SEM; JSM-IT200(A), Japan). The elemental analysis of the B_4C-TiB_2 composite ceramics was obtained by energy dispersive spectroscopy (EDS; JSM-IT200(A), Japan). The hardness of the B_4C-TiB_2 composite ceramics was measured by a Vickers hardness tester (KB5-BVZ, Germany) with an applied load of 0.98–49 N for 10 s on the polished surface. The electrical performance was measured by a Hall effect measurement system (ECOPIA/HMS-5500, Korea). The shear and longitudinal velocities were measured by an ultrasound measurement system (OWON, 5072PR, China) to calculate Young's modulus, and then fracture toughness was calculated based on the indentation crack length.

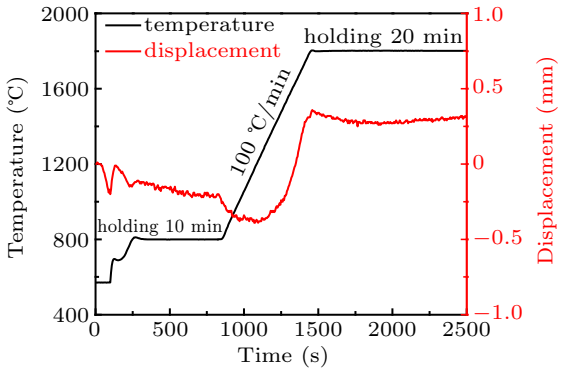


Fig. 3. The temperature and displacement change at 1800 °C with SPS.

3. Results and discussion

3.1. Density and phase compositions

The densities of $B_4C + x$ wt% TiH_2 ($x = 0$, 5, 10, 15, 20) sintered at 1400 °C, 1500 °C, 1600 °C, 1700 °C, and 1800 °C are shown in Table 1. At 1900 °C sintering, the sample began to melt out of the sintering range, and the mechanical and electrical properties of B_4C + TiB_2 composite ceramics were the best when sintering at 1800 °C. On this basis, 0–20 wt% TiH_2 were added to further optimize its performance.

Table 1. Density of monolithic B_4C sintered from 1400 °C to 1800 °C.

Temperature (°C)	0 wt%	5 wt%	10 wt%	15 wt%	20 wt%
1400	2.20	1.83	1.85	2.04	2.06
1500	2.23	2.12	2.03	2.34	2.28
1600	2.27	2.25	2.17	2.54	2.51
1700	2.42	2.36	2.51	2.59	2.52
1800	2.51	2.57	2.62	2.74	2.83

The results showed that the pure B_4C ceramic reached complete densification at 1800 °C (the theoretical density of B_4C is 2.51 g·cm^{-3}). Figure 4 shows the density of B_4C ceramics sintered with different TiH_2 content at 1800 °C,[27] with increasing TiH_2 content, the density of the composite ceramic reached a maximum at 20 wt% TiH_2. Both TiB_2 and C can reduce the sintering temperature and inhibit the grain growth. Because TiB_2 has a relatively low crystalline boundary diffusion coefficient, which promotes slow densification,[28] graphite (C) has a binding effect on the grain boundary, which can enhance grain bounding diffusing and fast densification. Therefore, the B_4C-TiB_2 composite ceramics are densified well.

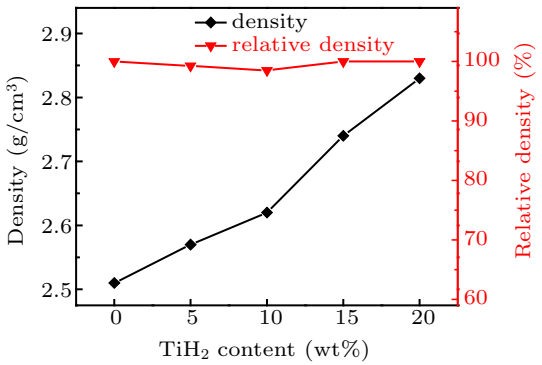


Fig. 4. Density of B_4C specimens as a function of (0–20) wt% TiH_2 content at 1800 °C.

Figure 5 shows the XRD analysis of the B_4C-TiB_2 composite ceramics doped with different TiH_2 content and sintered at 1800 °C for 20 min. With increasing TiH_2 content, the intensity of the TiB_2 diffraction peaks (around 44°) continued to increase and reached a maximum with 20 wt% TiH_2.[29] Due to the decomposition of TiH_2 powder at 620 °C via the process shown in Eq. (1), the temperature was maintained at 800 °C for 10 min to ensure the complete formation of Ti. B_4C is divided into B and C through the process shown in Eq. (2), the presence of element C in the XRD pattern also confirms this statement. Ti and B form TiB_2 through the process shown in Eq. (3). The results indicated that an appropriate ratio of B_4C and TiH_2 could be completely converted into B_4C-TiB_2 ceramics through the process shown in Eq. (4) after sintering by SPS in a high vacuum environment. In this experiment, TiB_2 was generated by the *in situ* reaction of B_4C and TiH_2, which can be described by the following three equations:

$$TiH_2 \rightarrow Ti + H_2, \tag{1}$$

$$B_4C \rightarrow 4B + C, \tag{2}$$

$$Ti + 2B \rightarrow TiB_2. \tag{3}$$

The overall reaction can be summarized as follows:

$$B_4C + 2TiH_2 = 2TiB_2 + C + 2H_2\uparrow. \tag{4}$$

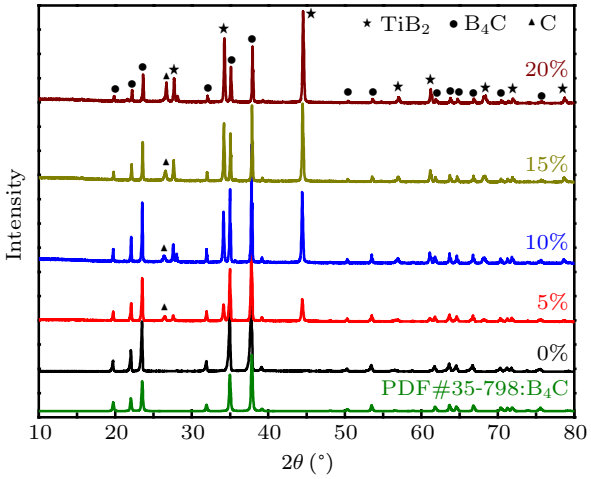


Fig. 5. XRD patterns of the synthesized $B_4C + x$ wt% TiH_2 ($x = 0$, 5, 10, 15, 20) composite ceramics.

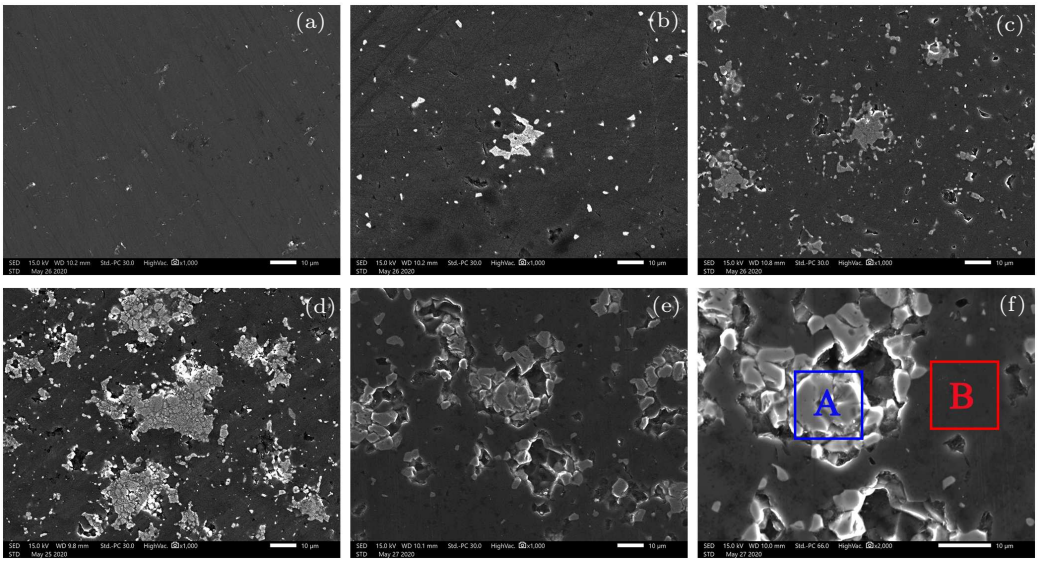


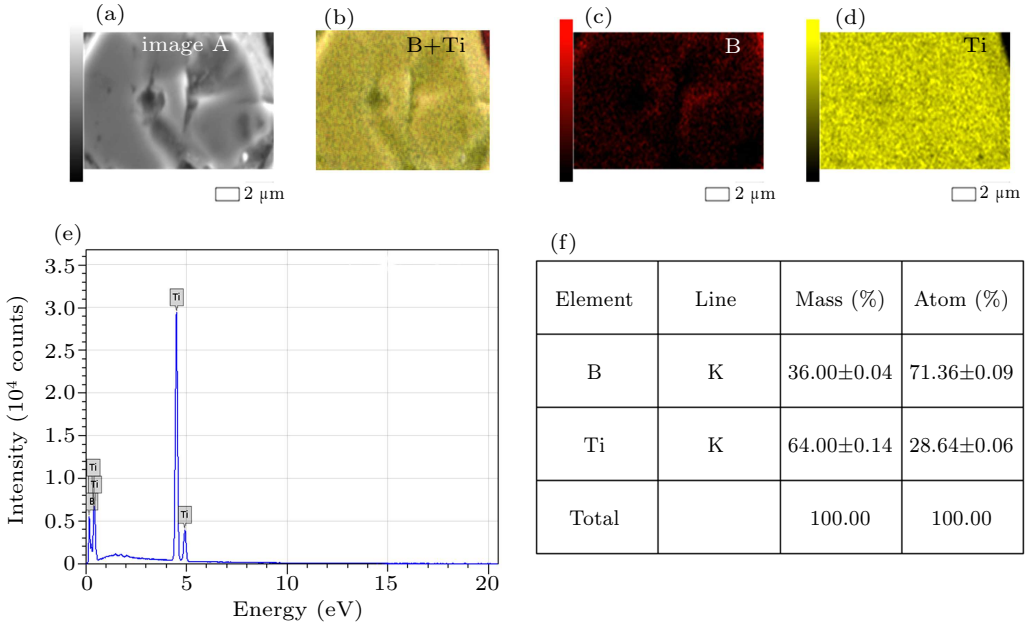
Fig. 6. Polished surfaces of B_4C ceramics sintered with different amount of TiH_2 at 1800 °C. (a) B_4C-0 wt% TiH_2; (b) B_4C-5 wt% TiH_2; (c) B_4C-10 wt% TiH_2; (d) B_4C-15 wt% TiH_2; (e) B_4C-20 wt% TiH_2. (f) The enlarged view of B_4C-20 wt% TiH_2, the blue (A) and red (B) squares are EDS regions.

Figures 6(a)–6(f) show the images of the microstructure of B_4C-TiB_2 composite ceramics containing different TiH_2 content. The content of second-phase TiB_2 increased with increasing TiH_2 content. It was supposed that Ti originally existed at the brighter areas, and then the melted Ti reacted with B to form TiB_2 *in situ* during sintering. Grain growth was not obvious in the B_4C matrix as it was inhibited by the reaction of second-phase TiB_2. When the content of TiH_2 was increased to 20 wt%, large-sized TiB_2 grains of about 3–4 μm appeared with inhomogeneous distribution in the microstructure, as shown in Fig. 6(e), these could aggregate into 30–40 μm grains. The reaction between Ti and B is highly exothermic in behavior and the heat generated helps to accelerate the formation of TiB_2 readily. The primary TiB_2 particles

on the surface of B_4C are appreciably free and movable and because of boron diffusion across boundary layer, TiB_2 particles grow with the primary ones forming agglomerates.[30]

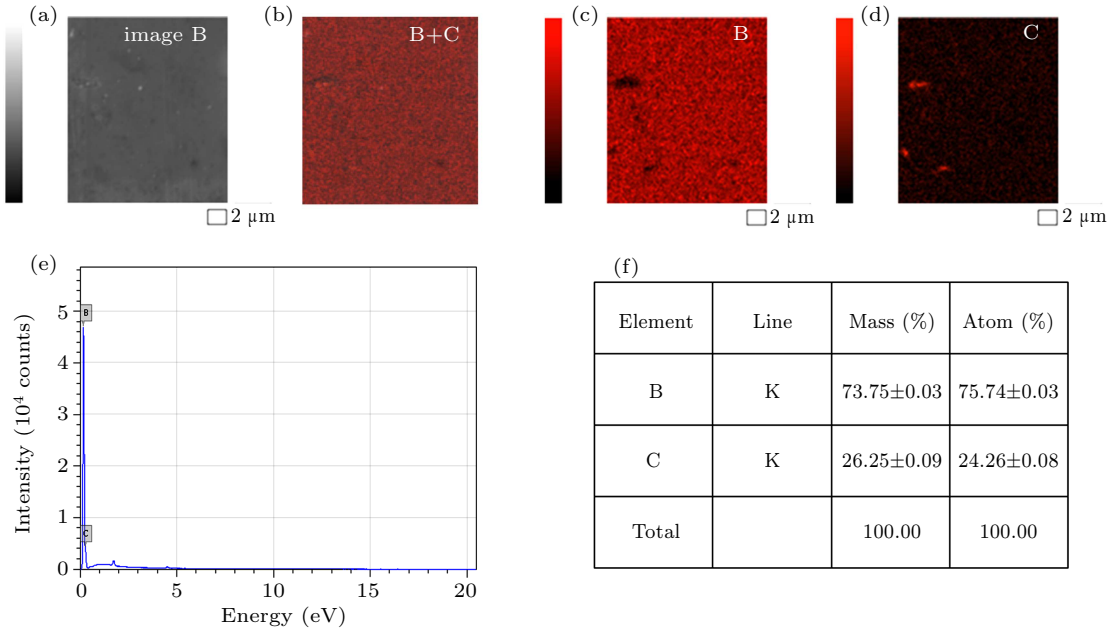
Figure 7 shows the results of EDS of part A in Fig. 6(f). Figure 7(a) is an enlarged image of A, and the elemental content and distribution of A are shown in Figs. 7(b)–7(f). XRD results combined with EDS spectra confirmed the phase distribution and that the light grey phase[31] was TiB_2, which has excellent electrical conductivity.

Figure 8 shows the EDS analysis of part B in Fig. 6(f). Figure 8(a) is an enlarged image of B, and the elemental content and distribution of B are shown in Figs. 8(b)–8(f). XRD results combined with EDS spectra confirmed that the phase distribution of the matrix was B_4C, which has poor electrical conductivity.



Element	Line	Mass (%)	Atom (%)
B	K	36.00±0.04	71.36±0.09
Ti	K	64.00±0.14	28.64±0.06
Total		100.00	100.00

Fig. 7. The related EDS spectra of blue A in Fig. 6(f) sintered with 20 wt% of TiH_2 at 1800 °C. (a) EDS test area image A; (b) titanium-K, boron-K; (c) boron-K; (d) titanium-K; (e) EDS spectra of image A; (f) element content of image A.



Element	Line	Mass (%)	Atom (%)
B	K	73.75±0.03	75.74±0.03
C	K	26.25±0.09	24.26±0.08
Total		100.00	100.00

Fig. 8. The related EDS spectra of red B in Fig.6 (f) sintered with 20 wt% of TiH_2 at 1800 °C. (a) EDS test area image B; (b) boron-K, carbon-K; (c) boron-K; (d) carbon-K; (e) EDS spectra of image B; (f) element content of image B.

3.2. Hardness and fracture toughness

The mechanical properties of B_4C-TiB_2 were measured on the polished surface, as displayed in Fig. 9.[32,33] The hardness-load curve of B_4C-20 wt% TiH_2 is shown in Fig. 9(a), revealing the obvious decrease in Vickers hardness (H_V) with increasing applied force, which was primarily attributed to the indentation size effect. An asymptotic H_V value

of ~ 31.4 GPa was obtained when the applied load exceeded 49 N. It may be because the hardness of TiB_2 generated by the reaction is 34 GPa, and the hardness of C produced by the reaction is poor, whose hardness is 1–2 GPa,[34,35] and the hardness of B_4C is 31 GPa, which is between those of TiB_2 and C. However, the results indicated that due to very little C produced by the reaction, the hardness of B_4C-TiB_2 composite ceramics did not decrease under the combined action of TiB_2 and C. Vickers hardness and fracture toughness results for the B_4C-TiB_2 composite ceramics are shown in Fig. 9(b). When doped with 20 wt% TiH_2, the hardness of the sample was stable and the fracture toughness was a maximum of 8.5 MPa·m$^{1/2}$. TiB_2 is a high-toughness material, and C also can be used as an additive to produce high-toughness ceramic,[36–39] so the fracture toughness of B_4C-TiB_2 composite ceramics is improved.

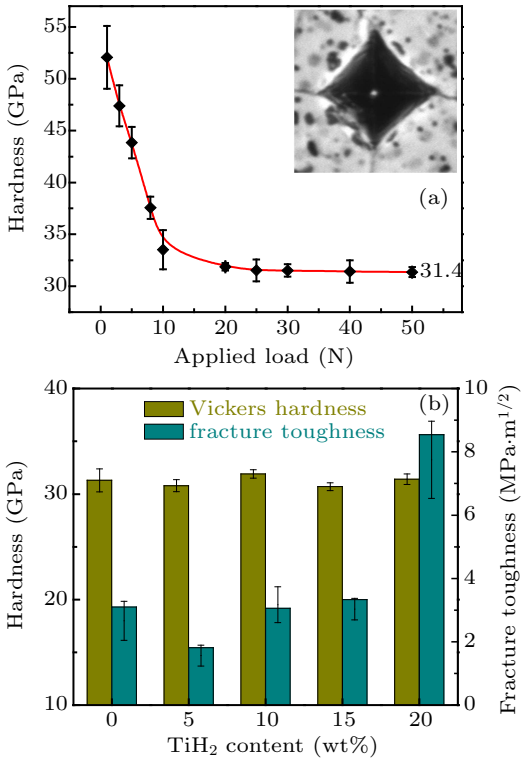


Fig. 9. Comparison of mechanical properties. (a) The measured Vickers hardness of B_4C-20 wt% TiH_2 up to 49 N load at 1800 °C. (b) Effect of TiH_2 addition on the hardness and fracture toughness of B_4C at 1800 °C.

To calculate the fracture toughness, an oscilloscope was used to measure the shear and longitudinal wave sound velocities and then the Poisson ratio μ was calculated using Eq. (5). Data for the Young's modulus calculation was then obtained using Eq. (6). Finally, the fracture toughness of the B_4C-TiB_2 composite ceramics was calculated according to Eq. (7).

The crack trace of the polished surface of the 20 wt% TiH_2 composite ceramic is shown in Fig. 10. Crack bridging, crack deflection, crack bending, and crack forking occurred when a force was applied, and these cracks acted as tougheners for consuming energy. Crack bridging is helpful to improve fracture toughness.[40] The following three formulas were applied to calculate the fracture toughness:

$$\mu = \frac{\frac{1}{2}\left(\frac{V_L}{V_T}\right)^2 - 1}{\left(\frac{V_L}{V_T}\right)^2 - 1}, \tag{5}$$

$$E = \frac{V_L^2 \times \rho \times (1-\mu) \times (1-2\mu)}{1-\mu}, \tag{6}$$

$$K_{IC} = 0.016 \times \left(\frac{E}{H_V}\right)^{\frac{1}{2}} \times \frac{P}{C^{3/2}}. \tag{7}$$

The factors affecting fracture toughness are density, hardness, sound velocity, and so on. Under the condition of constant hardness, B_4C-TiB_2 composite ceramic had the maximum density at 20 wt% TiH_2 doping, which can improve the fracture toughness. At the same time, grain size also affected the sound velocity of the B_4C-TiB_2 composite ceramic. Under the action of various factors, the fracture toughness of the B_4C-TiB_2 composite ceramic reached 8.7 MPa·m$^{1/2}$.

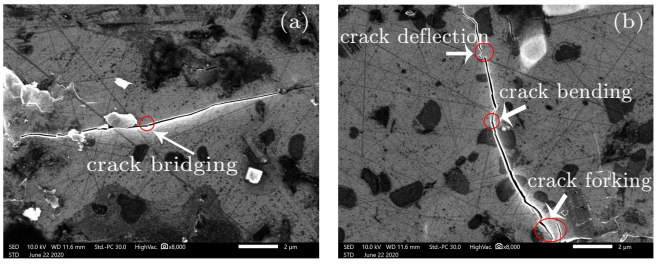


Fig. 10. SEM micrographs of the polished surfaces cracks of the B_4C-TiB_2 composite ceramics with 20 wt% TiH_2.

3.3. Electrical conductivity

The electrical conductivity of the $B_4C + x$ wt% TiH_2 (x = 0, 5, 10, 15, 20) composite ceramics at different sintering temperatures (1400 °C, 1500 °C, 1600 °C, 1700 °C, and 1800 °C) is shown in Fig. 11. The electrical conductivity could be enhanced by increasing the sintering temperature and increasing the content of TiH_2. When doped with 5 wt% or 10 wt% TiH_2, the electrical conductivity of the B_4C-TiB_2 composite ceramics suddenly increased. When TiH_2 was further increased to 15 wt% or 20 wt%, the electrical conductivity of the B_4C-TiB_2 composite ceramics was two orders of magnitude higher than that of pure B_4C. At room temperature, a maximum electrical conductivity of 114.9 S·cm^{-1} was achieved with 20 wt% TiH_2. Graphite is one type of carbon-based filler, due to being layered structure, its electrical conductivity is 10^4 S/cm at room temperature.[41] Ti reacted with B to form TiB_2, the layered structure of boron atoms similar to graphite and the outer electrons of Ti determine the outstanding electrical conductivity of TiB_2, they can be used for improving the electrical conductivity of composite ceramics.

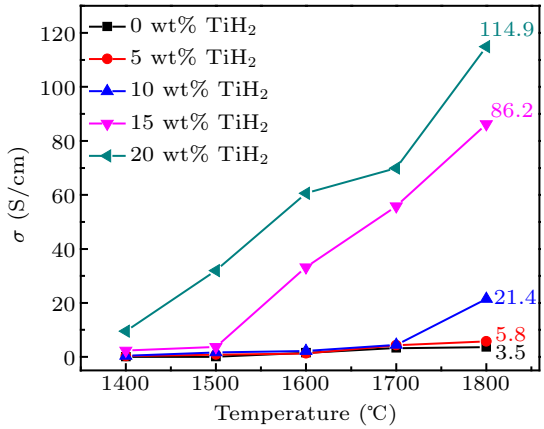


Fig. 11. The electrical conductivity of B_4C-(0, 5, 10, 15, 20) wt% TiH_2 composite ceramics at different sintering temperature.

4. Conclusion

Completely densified B_4C-TiB_2 composite ceramics with high conductivity, high strength, and high hardness properties were successfully obtained by the spark plasma sintering method starting from raw mixtures of B_4C and TiH_2 powders. Using TiH_2 as a sintering aid improved the density of the B_4C ceramics. During the sintering process, B_4C reacted with Ti to form TiB_2 and a small amount of C, which successfully inhibited the growth of B_4C and improved the electrical conductivity, Young modulus, and fracture toughness.

References

[1] An L Q, Wang L Y, Wang L F, Fan R H, Ito A and Goto T 2020 *J. Eur. Ceram. Soc.* **40** 4589
[2] Grigoriev S N, Volosova M A, Peretyagin P Y, Seleznev A E, Okunkova A A and Smirnov A 2018 *Appl. Sci.* **8** 2385
[3] Domnich V, Reynaud S, Haber R A and Chhowalla M 2011 *J. Am. Ceram. Soc.* **94** 3605
[4] Jamale S and Kumar B V M 2020 *Int. J. Refract. Met. H* **87** 105124
[5] Wang C C and Song L L 2019 *Chin. Phys. B* **28** 066201
[6] Sarithadevi H V, Swapna M S, Ambadas G and Sankararaman S 2018 *Chin. Phys. B* **27** 107702
[7] He Y, Shen Y D, Tang B and An Q 2020 *J. Eur. Ceram. Soc.* **40** 4428
[8] Zhang W, Yamashita S and Kita H 2019 *Adv. Appl. Ceram.* **118** 222
[9] Badica P, Grasso S, Borodianska H, Xie S S, Li P F, Takarko P, Reece M J, Sakka Y and Vasylkiv O 2014 *J. Ceram. Soc. Jpn.* **122** 271
[10] Sairam K, Sonber J K, Murthy T S R C, Subramanian C, Fotedar R K, Nanekar P and Hubli R C 2014 *Int. J. Refract. Met. H* **42** 185
[11] Singh P, Singh B, Kumar M and Kumar A 2014 *Ceram. Int.* **40** 15331
[12] Moskovskikh D O, Paramonov K A, Nepapushev A A, Shkodich N F and Mukasyan A S 2017 *Ceram. Int.* **43** 8190
[13] Heydari M S and Baharvandi H R 2015 *Int. J. Refract. Met. H* **51** 224
[14] Heydari M S and Baharvandi H R 2015 *Int. J. Refract. Met. H* **51** 61
[15] White R M and Dickey E C 2014 *J. Eur. Ceram. Soc.* **34** 2043
[16] Gao Y B, Tang T G, Yi C H, Zhang W, Li D C, Xie W B, Huang W and Ye N 2016 *Mater. Design.* **92** 814
[17] He Q L, Wang A Y, Liu C, Wang W M, Wang H and Fu Z Y 2018 *J. Eur. Ceram. Soc.* **38** 2832
[18] Yue X Y, Zhao S M, Lu P, Chang Q and Ru H Q 2010 *Mat. Sci. Eng. A-Struct.* **527** 7215
[19] White R M, Kunkle J M, Polotai A V and Dickey E C 2011 *J. Eur. Ceram. Soc.* **31** 1227
[20] Karimoto T and Nishimoto A 2019 *Mater. Trans.* **60** 2387
[21] Shi S F, Cho S H, Goto T and Sekino T 2018 *J. Am. Ceram. Soc.* **101** 3181
[22] Chu K, Liu Z F, Jia C C, Chen H, Liang X B, Gao W J, Tian W H and Guo H 2010 *J. Alloy. Compd.* **490** 453
[23] Tan Y Q, Chen C, Li F Z, Zhang H B, Zhang G J and Peng S M 2015 *RSC. Adv.* **5** 76309
[24] Pan Y and Chen S 2020 *Int. J. Energ. Res.* **44** 4997
[25] Ito M, Setoyama D, Matsunaga J, Muta H, Kurosaki K, Uno M and Yamanaka S 2006 *J. Alloy. Compd.* **420** 25
[26] Liu H, He P, Feng J C and Cao J 2009 *Int. J. Hydrogen. Energ.* **34** 3018
[27] Rehman S S, Ji W, Khan S A, Fu Z Y and Zhang F 2015 *Ceram. Int.* **41** 1903
[28] Pei L Z and Xiao H N 2009 *J. Mater. Process. Tech.* **209** 2122
[29] Yin S P, Zhang Z H, Cheng X W, Su T J, Hu Z Y, Song Q and Wang H 2018 *Ceram. Int.* **44** 21626
[30] Suresh S and Moorthi N S V 2012 *Procedia. Eng.* **38** 89
[31] Wen Q, Tan Y Q, Zhong Z H, Zhang H B and Zhou X S 2017 *Mat. Sci. Eng. A-Struct.* **701** 338
[32] Anstis G R, Chantikui P, Lawn B R and Marshall D B 1981 *J. Am. Ceram. Soc.* **64** 533
[33] Ma D J, Wang J L and Sun L 2017 *J. Am. Ceram. Soc.* **100** 2296
[34] Sengupta R, Bhattacharya M, Bandyopadhyay S and Bhowmick A K 2011 *Prog. Polym. Sci.* **36** 638
[35] Oku T, Kurumada A, Imamura Y and Ishihara M 2008 *J. Nucl. Mater.* **381** 92
[36] Peng C, Tang H, He Y, Lu X Q, Jia P, Liu G Y, Zhao Y C and Wang M Z 2020 *J. Mater. Sci. Technol.* **51** 161
[37] Skorokhod V and Krstic V 2000 *J. Mater. Sci. Lett.* **19** 237
[38] Shi L, Li H Y, Zou Z M, Fok A S L, Marsden B J, Hodgkins A, Mummery P M and Marrow J 2008 *J. Nucl. Mater.* **372** 141
[39] Chen H H N, Su R K L, Fok S L and Zhang H G 2017 *Eng. Fract. Mech.* **186** 143
[40] Ouagne P, Neighbour G B and McEnaney B 2002 *J. Phys. D: Appl. Phys.* **35** 927
[41] Reis J M L, Martins S A and Costa Mattos H S D 2020 *J. Braz. Soc. Mech. Sci.* **42** 1045